2011 50th IEEE Conference on Decision and Control and
European Control Conference (CDC-ECC)
Orlando, FL, USA, December 12-15, 2011

Control-Oriented Modeling of the Electron Cyclotron Current Drive Actuated Hybrid Mode in ITER

Snezana Djordjevic, Maarten Steinbuch, Marco de Baar, Dick Hogeweij, and Jonathan Citrin

Abstract— **This paper presents a control-oriented model of the magnetic flux in the International Tokamak Experimental Reactor (ITER) actuated with Electron Cyclotron Current Drive (ECCD) at different locations. The main objective of the control-oriented modeling is to derive an input/output representation of the magnetic profile written as a state-space model. The state-space model allows determination of the most suitable actuation strategies using the concept of controllability analysis. To illustrate the controllability analysis of the magnetic flux actuated at different locations, we present numerical results based on space dependent parameters obtained from the integrated modeling code CRONOS.**

I. INTRODUCTION

With the latest developments towards the realization of the International Tokamak Experimental Reactor (ITER), nuclear fusion is about to demonstrate scientific feasibility of fusion energy production. At the present stage of ITER development, the fusion control strategy relies on the developments of previous tokamaks, e.g. Tore Supra and JET [1]. The control approaches developed for the previous tokamaks have shown that different control methods can be effectively used to improve the plasma performance. The performance of the plasma has been influenced through active modification of the current density and pressure profiles in advanced plasma regimes with Internal Transport Barriers (ITBs), through heating and current drive, and through sheared plasma rotation. The improvement of the plasma performance has been demonstrated on TFTR [2], JT-60U [3], and JET [4]. These results are mainly based on linear models identified from experiments [5], or on semi-empirical correlations which can be embedded in real-time control of plasmas [6]. More recently, a spatially distributed model of the q-profile and ψ-profile have been suggested in [7], which opens a new perspective on control of nuclear plasma. The development of different spatially distributed model-based control scenarios for operation of ITER can lead to a more efficient fusion energy production with minimal input energy.

In principle, a tokamak plasma is organized in axisymmetric flux-surfaces. These are nested tori of constant magnetic flux. Fieldlines are embedded in these surfaces. Furthermore, the transport along the fieldlines is "fast" and the surfaces thus feature constant temperature and particle density. Consequently, the transport problem can be reduced to a one-dimensional system in the direction perpendicular to the flux-surfaces. Using first principles transport based models under various assumptions, such as constant pedestal pressure, constant pedestal temperature, and stationary state resistivity, the phenomena inside ITER can be modeled as simplified spatially distributed systems [7]. The simplified transport models represent the flux diffusion models and include some key physical knowledge of the tokamak as well as the experimental results from JET and Tore Supra.

In this paper, we introduce a control-oriented model of the magnetic flux evolution which describes the magnetic flux in poloidal direction. The model is governed by a one-dimensional partial differential equation (PDE), which describes the spatial variation of the ψ-profile. The set of parameter estimations is motivated by the results presented in [7], where the core of the problem of modeling plasma dynamics, e.g. ψ-profile, is a type of convection-diffusion problem with parameters that connect the dynamics. In this work, we consider the current density generated by the Electron Cyclotron Current Drive (ECCD) as a spatially distributed input, whereas the other noninductive components of the current density distribution and the plasma resistivity are assumed to be spatially distributed parameters. The spatially distributed parameters are obtained from the integrated modeling code CRONOS [8]. In order to avoid the present long trial-and-error approach to deposite the contribution to the current from $j_{\mathrm{eccd}}(x)$, a more general actuator strategy for deposition of $j_{\mathrm{eccd}}(x)$ is needed to determine reachable and unreachable flux ψ-profiles. From the control perspective, the reachable and unreachable profiles represent the controllable and uncontrollable subspaces [9] in the proposed control-oriented model.

The paper is organized as follows: Section II presents the control-oriented model of the magnetic flux and its state-space model representation. Section III establishes the control problem related to the j_{eccd} deposition and the controllability analysis based on the controllability Gramian. Section IV draws the conclusions of the paper.

II. MAGNETIC FLUX

The general ITER principles rely on the tokamak concept of magnetic confinement, in which the plasma is contained in a doughnut-shaped vacuum vessel. Control methods are required in ITER both to maintain plasma stability, and also to optimize the energy efficiency of the burning plasma. For a given plasma density, the fusion power is primarily

Snezana Djordjevic, Maarten Steinbuch, and Marco de Baar are with Eindhoven University of Technology, Faculty of Mechanical Engineering, Control Systems Technology, PO Box 513, 5600 MB Eindhoven, The Netherlands S.Djordjevic@tue.nl

Marco de Baar, Dick Hogeweij, and Jonathan Citrin are with FOM-Institute for Plasma Physics Rijnhuizen, Association EURATOM-FOM, Trilateral Euregio Cluster, P.O. Box 1207, 3430 BE Nieuwegein, The Netherlands

978-1-61284-799-3/11/$26.00 ©2011 IEEE

TABLE I

PHYSICAL VARABLES.

Variables	Physical meaning	Units
T_i	ion temperature	eV
$T_{\rm ped}$	pedestal temperature	eV
q	safety factor	
s	magnetic shear	
ψ	magnetic flux of the poloidal field	T/m
$B_{\rm pol}$	magnetic field in poloidal direction	T
S	surface	$\rm m^2$
$\eta_\parallel$	plasma resistivity	$\Omega\times$m
μ_0	permeability of free space	H/m
a_e	minor radius	m
R_0	major radius	m
I_p	total plasma current	A
$j_{\rm ni}$	noninductive effective current density	$\rm A/m^2$
$j_{\rm bc}$	bootstrap current density	$\rm A/m^2$
$j_{\rm nbi}$	current density driven by the neutral beams	$\rm A/m^2$
$j_{\rm eccd}$	current density driven by the ECCD	$\rm A/m^2$

determined by the ion temperature T_i profile. Control of the T_i profile, at the same input power into the tokamak, is thus key to optimizing tokamak energy efficiency. In many cases, the T_i profile stays close to the critical gradient for the onset of turbulent, ion temperature gradient (ITG) driven, transport, which satisfies in the flat limit $(\nabla T_i/T_i)_{\rm crit} = 4/3(T_i/T_e)\cdot(1+2s/q)$, where q is the safety factor and s is the magnetic shear [10], [11]. Assuming that indeed $(\nabla T_i/T_i) = (\nabla T_i/T_i)_{\rm crit}$, and assuming a given value for $T_{{\rm ped},i}$, the T_i profile can be expressed as a function of s/q, which in turn is a function of the poloidal magnetic flux $\psi(x,t)$, where x is a normalized one-dimensional radial coordinate. This means that the poloidal magnetic flux $\psi(x,t)$ can be indirectly used to shape the ITER T_i profile.

A. Control-Oriented Model of the Magnetic Flux

The poloidal magnetic flux $\psi(x,t)$ is the total flux through the surface S defined by a circle centered on the toroidal axis, whose edge coincides with the flux surface related to the coordinate x, as illustrated in Figure 1. The magnetic flux through the surface is given as

$$\psi(x,t) = \frac{1}{2\pi}\int B_{\rm pol} dS.$$

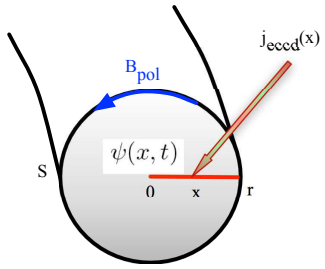

Fig. 1. Deposition of $j_{\rm eccd}(x)$ centered on the flux surface defined by the coordinate x.

This means that the poloidal flux $\psi(x,t)$ can be indirectly used to shape the magnetic field in poloidal direction $B_{\rm pol}$.

Using cylindrical approximation for the domain $r\in[0,a]$, with $x{\equiv}r/a$ and neglecting the diamagnetic effect, the following flux profile evolution can be derived as suggested in [7]

$$\frac{\partial\psi(x,t)}{\partial t} = \frac{\eta_\parallel(x)}{\mu_0 a_{\rm e}^2}\left(\frac{\partial^2\psi(x,t)}{\partial x^2} + \frac{1}{x}\frac{\partial\psi(x,t)}{\partial x}\right) + \eta_\parallel(x)R_0 j_{\rm ni}(x,t), \quad (1)$$

where

$$j_{\rm ni}(x,t) = j_{\rm bc}(x) + j_{\rm nbi}(x) + j_{\rm eccd}(x,t). \quad (2)$$

The notations and units of the main physical variables are summarized in Table I.

In this case, where the magnetic flux is modeled as a diffusion effect, the boundary conditions have to be specified both at the plasma center and at the last closed magnetic surface (LCMS). At the center of the plasma, the spatial variation of the flux is zero, i.e.

$$\frac{\partial\psi(0,t)}{\partial x} = 0, \quad (3)$$

and at the LCMS

$$\frac{\partial\psi(1,t)}{\partial x} = -\frac{R_0\mu_0 I_p}{2\pi}. \quad (4)$$

Note that the model (1) is scaled. This allows us to examine the plasma properties regardless of the size of future tokamaks. Rescaling can be easily done using a large amount of experimental data available from actual tokamakas, specific engineering parameters, and scaling laws [7].

B. Spatially Distributed Parameters

In (1), we assume $\eta_\parallel(x)$, $j_{\rm bc}(x)$, and $j_{\rm nbi}(x)$ to be the space dependent system parameters. The space dependent parameters are obtained from CRONOS for three different stationary state regimes at $T_{\rm ped} = 3$keV, $T_{\rm ped} = 4$keV, and $T_{\rm ped} = 5$keV, with constant plasma current $I_p = 1.2\cdot10^7$A.

1) Plasma resistivity $\eta_\parallel(x)$: Figure 2 shows the space variation of the plasma resistivity for all three different stationary state regimes. As illustrated, the plasma resistivity

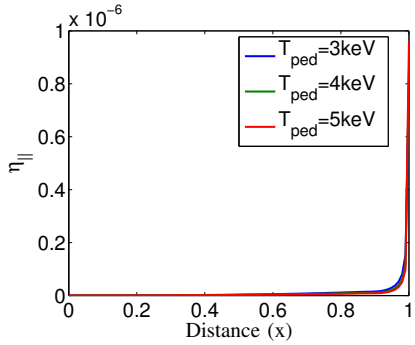

Fig. 2. Plasma resistivity profiles in the stationary state regimes at $T_{\rm ped}$ at 3keV, 4keV, and 5keV.

becomes more dominant at the LCMS for the chosen T_{ped}. The chosen stationary state regimes have minor or almost no influence on the plasma resistivity. This supports our decision for choosing the plasma resistivity $\eta_{\parallel}(x)$ to be the space dependent system parameter.

2) Bootstrap current density $j_{\text{bc}}(x)$: The bootstrap current density $j_{\text{bc}}(x)$ is usually generated by trapped particles and represents the noninductive current in this specific scenario [11].

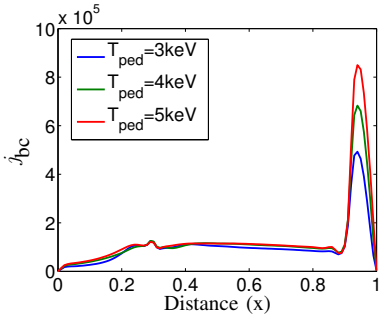

Fig. 3. Bootstrap current density profiles in the stationary state regimes at T_{ped} at 3keV, 4keV, and 5keV.

In this work, we also consider the bootstrap current density profile of $j_{\text{bc}}(x)$ to be the spatially distributed parameter as illustrated in Figure 3. The $j_{\text{bc}}(x)$ profiles show almost no variations with respect to space, except for the region between $x = 0.9$ and $x = 1$ where the variations are evident due to the pedestal height.

3) Current density $j_{\text{nbi}}(x)$: The non-negligible influence of T_{ped} on the neutral beam current density profiles can be observed by comparing the $T_{\text{ped}} = 4$keV and 5keV cases in Figure 4. The greater difference for the $T_{\text{ped}} = 3$keV case is due to reduced NBI power prescribed in the $T_{\text{ped}} = 3$keV scenario. Figure 4 illustrates the influence of T_{ped} on the $j_{\text{nbi}}(x)$ profiles.

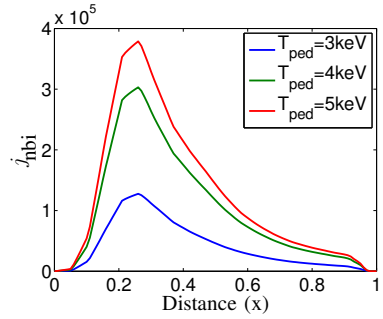

Fig. 4. Current density profiles driven by the neutral beams in the stationary state regimes at T_{ped} at 3keV, 4keV, and 5keV.

C. Spatially Discretized Model

Due to the fact that the parameters $\eta_{\parallel}(x)$, $j_{\text{bc}}(x)$, and $j_{\text{nbi}}(x)$ are space dependent parameters, the PDE model (1) has to be discretized in order to evaluate the magnetic flux $\psi(x,t)$. Considering the dynamics obtained in (1), a spatially discretized model can be obtained according to the chosen numerical scheme as follows

$$\frac{\mathrm{d}\psi_{\mathrm{i}}(\mathrm{t})}{\mathrm{dt}} = \frac{\eta_{\parallel_{i,j}}}{\mu_0 a_e^2}\left(c_1(i)\psi_{i+1}(t) - c_2(i)\psi_i(t) + c_3(i)\psi_{i-1}(t)\right) + \eta_{\parallel_{i,j}} R_0\left(j_{\mathrm{bc,i}} + j_{\mathrm{nbi,i}} + j_{\mathrm{eccd,i}}(t)\right), \tag{5}$$

with the discretization coefficients

$$c_1(i) = 1/2\,\frac{2\,x_i + \delta x}{\delta x^2 x_i},$$
$$c_2(i) = 2\,\frac{1}{\delta x^2},$$
$$c_3(i) = 1/2\,\frac{2\,x_i - \delta x}{\delta x^2 x_i},$$

where the index i denotes the discretization point in space, $i = 1, 2, ..., N$, and δx represents the characteristic length of the cell defined between two spatial discretization points [7]. For the sake of simplicity, we consider here a finite difference explicit method on a piecewise equidistant mesh with constant $\delta x = \text{const}$. The parameter estimation at each point i for $\eta_{\parallel}(x)$, $j_{\mathrm{bc,i}}$, and $j_{\mathrm{nbi,i}}$ are obtained from the CRONOS code previously discussed, whereas the $j_{\mathrm{eccd,i}}(t)$ profile is considered to be the manipulated variable.

Boundary condition at the center: The flux at the center equals zero, which gives the following expression for ψ_1

$$\frac{\psi_1 - \psi_0}{\delta x} = 0 \quad \rightarrow \quad \psi_0 = \psi_1$$

so that the ODE equation for $\psi_1(t)$ reads as

$$\frac{d\psi_1(t)}{dt} = \frac{\eta_{\parallel_{i,j}}}{\mu_0 a_e^2}\left((c_3(1) - c_2(1))\psi_1(t) + c_1(1)\psi_2(t)\right) + \eta_{\parallel_{i,j}} R_0\left(j_{\mathrm{bc,1}} + j_{\mathrm{nbi,1}} + j_{\mathrm{eccd,1}}(t)\right).$$

Boundary condition at the edge: The fact that the flux at LCMS is a constant value written as a function of I_p (4)

$$\frac{\psi_{N+1} - \psi_N}{\delta x} = -\frac{R_0 \mu_0 I_p}{2\pi},$$

gives the following dynamics at the edge

$$\frac{d\psi_N(t)}{dt} = \frac{\eta_{\parallel_{i,j}}}{\mu_0 a_e^2}\left[(c_1(N) - c_2(N))\psi_N(t) - c_1(N)\psi_{N-1}(t)\right) + \frac{\eta_{\parallel_{i,j}}}{\mu_0 a_e^2}\delta x c_1(N) + \eta_{\parallel_{i,j}} R_0\left(j_{\mathrm{bc,N}} + j_{\mathrm{nbi,N}} + j_{\mathrm{eccd,N}}(t)\right].$$

Now that we have a fully discretized model with the boundary conditions embodied, we can define an input/output structure using the discretized $\psi_i(t)$ profile as states

$$\psi_i(t) = \begin{bmatrix} \psi_1(t) \\ \psi_2(t) \\ \psi_3(t) \\ \vdots \\ \psi_N(t) \end{bmatrix},$$

and the boundary condition at the edge and the current density profiles as inputs $\mathbf{u}$(t)

$$\mathbf{u}(t) = \begin{bmatrix} \psi_{bc} & 0 & 0 & 0 \\ 0 & j_{\mathrm{eccd,i}}(t) & 0 & 0 \\ 0 & 0 & j_{\mathrm{nbi,i}} & 0 \\ 0 & 0 & 0 & j_{\mathrm{bc,i}} \end{bmatrix}.$$

The state-space representation of the proposed spatially discretized model (5) is

$$\frac{\mathrm{d}\psi_{\mathrm{i}}(\mathrm{t})}{\mathrm{dt}} = \mathbf{A}\psi_i(t) + \mathbf{B}\mathbf{u}(t) \quad (6)$$

$$y_i(t) = \mathbf{C}\psi_i(t) \quad (7)$$

where $\psi_i(t) \in \mathbb{R}^N$ is the state vector, $\mathbf{u} \in \mathbb{R}^{4\times 4}$ is the input matrix with the system matrix $\mathbf{A} \in \mathbb{R}^{N\times N}$, and the input matrix $\mathbf{B} = \begin{bmatrix} \mathbf{B}_{11} & \mathbf{B}_{12} & \mathbf{B}_{13} & \mathbf{B}_{14} \end{bmatrix} \in \mathbb{R}^{N\times 4}$, with the output vector $y_i(t) \in \mathbb{R}^N$ and the output matrix $\mathbf{C} \in \mathbb{R}^{N\times N}$. We assume that the output vector $y_i = \mathbf{I}\psi_i(t)$, which means that the output matrix is the identity matrix $\mathbf{I}$ of order N. The placement of the current density $j_{\mathrm{eccd,i}}(t)$ is fully determined by the input matrix $\mathbf{B}_{12}$, where the position of the peak x corresponds to the current density $j_{\mathrm{eccd}}(x)$. Note also that the boundary condition at the LCMS and $j_{\mathrm{nbi,i}}$ and $j_{\mathrm{bc,i}}$ are also written as the inputs although they are not considered as manipulated variables with respect to time.

D. Actuation Strategies

As previously discussed, the main input is the noninductive current driven by the ECCD system $j_{\mathrm{eccd}}(x)$. The current density $j_{\mathrm{eccd}}(x)$ can be roughly modeled with Gaussian curves that have location of the peaks x and width of the distributions according to the following equation

$$j_{\mathrm{eccd}}(x) = \vartheta_{\mathrm{cd}} \mathrm{e}^{(-\mu_{\mathrm{cd}}-x)^2/2\sigma},$$

with the mean and the variance, respectively

$$\mu_{\mathrm{cd}} = \frac{\rho(R_{\mathrm{abs}})}{a} \quad \text{and} \quad \sigma_{\mathrm{cd}} = -\frac{(\mu_{\mathrm{cd}} - \rho(\mathrm{R_c})/\mathrm{a})^2}{2\ln\beta},$$

where β is chosen such that $j_{\mathrm{eccd}}(x_c) = \vartheta\beta \approx 0$ [7]. This is equivalent to setting the Gaussian curve close to zero at R_c.

The shape of the Gaussian distribution depends on the global plasma parameters and power inputs, which are the main drive forces of the magnetic flux inside ITER [11]. The maximum value of the current deposit can be computed from

$$\vartheta_{\mathrm{cd}} = \frac{\gamma P_{\mathrm{cd}}}{R_0 \overline{n}} \left(2\pi a^2 \int_0^1 x e^{(-\mu_{\mathrm{cd}}-x)^2/2\sigma} dx \right)^{-1}.$$

Figure 5 illustrates three different actuation strategies where the peak x is placed at the following locations: $x = 0.3$, $x = 0.35$, and $x = 0.4$. The influence of these different actuation strategies on the overall system behavior can be observed through the input matrix $\mathbf{B}$ according to the spatially discretized model written in the state-space form (6)-(7). Figure 5(b) shows the images of $\mathbf{B}_{12}$ for the chosen actuation strategies. The area that shows the non-zero entries in the input matrix $\mathbf{B}_{12}$ can be easily seen in Figure 5(b) through the red area in the image, whereas the zero entries are colored in blue. Changing the position of the j_{eccd} deposition changes the input matrix $\mathbf{B}_{12}$ and consequently influences the controllability of the magnetic flux $\psi_i(t)$.

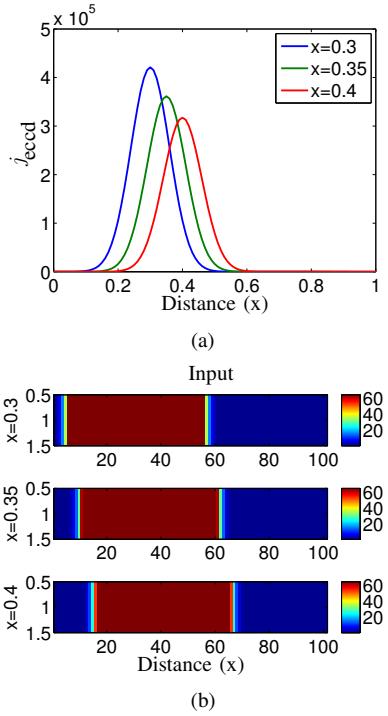

Fig. 5. Current density profiles driven by the ECCD (a) in space and (b) the space images at $x = 0.3$, $x = 0.35$, and $x = 0.4$ with the ECCD power 30MW at $T_{\mathrm{ped}} = 3\mathrm{keV}$.

III. CONTROL PROBLEM

In the presented control-oriented model, the current density $j_{\mathrm{eccd,i}}(t)$ is considered to be the spatially distributed input, whereas the output $y_i(t)$ can be considered to be the magnetic flux $\psi_i(t)$ in the entire domain x. For this input/output representation of the magnetic flux, the control problem can be formulated as finding the most suitable input strategy to reach desirable sets of $\psi_i(t)$ by placing $j_{\mathrm{eccd,i}}(t)$ at the most suitable location. To determine the most suitable location for $j_{\mathrm{eccd,i}}(t)$ deposition, we will introduce a controllability analysis for the state-space model given as (6)-(7).

A. Controllability and Observability Gramians

This section discusses different spatially distributed actuation strategies for the $j_{\mathrm{eccd}}(x)$ deposition using the following notion for the controllable subspace $\mathbb{X}^{\mathrm{con}}$

$$\mathbb{X}^{\mathrm{con}} = \mathrm{im}\left(\mathcal{C}(\mathbf{A}, \mathbf{B})\right) \subset \mathbb{R}^{\mathrm{N}} \quad (8)$$

where the controllability matrix $\mathcal{C}$ equals

$$\mathcal{C}(\mathbf{A}, \mathbf{B}) = \begin{bmatrix} \mathbf{B} & \mathbf{AB} & \mathbf{A}^2\mathbf{B} & \ldots & \mathbf{A}^{i-1}\mathbf{B} \end{bmatrix}. \quad (9)$$

The system is controllable if the controllability matrix has full rank. According to the Cayley-Hamilton theorem [12], the rank of $\mathcal{C}$ and its image are determined by the first $N \times N$

columns, where N is the state dimension which agrees with the number of discretization points in the x direction. For large scale systems, where $N > 10$, there are elements of $\mathbb{X}^{\text{con}}$ that require a significant amount of energy in terms of

$$\sum_{i=0}^{\infty} \mathbf{u}(t)^T \mathbf{u}(t)$$

in order to be reached [13]. The reachable and unreachable sets can be quantified using the controllability Gramian $\mathcal{P}$

$$\mathcal{P} = \mathcal{C}_\infty(\mathbf{A},\mathbf{B})\mathcal{C}_\infty^T(\mathbf{A},\mathbf{B}) = \sum_{i=0}^{\infty} \mathbf{A}^i \mathbf{B}\mathbf{B}^T (\mathbf{A}^T)^i, \qquad (10)$$

where $\mathcal{P} \in \mathbb{R}^{N\times N}$. The elements in $\mathbb{X}^{\text{con}}$, which require the most energy to be reached, have a significant component in the span of the eigenvectors of $\mathcal{P}$ corresponding to small absolute eigenvalues [14].

Similar to the concept of input energy, there are elements that produce more energy in terms of outputs and observable subspaces

$$\sum_{i=0}^{\infty} y_i(t)^T y_i(t)$$

according to the observability matrix $\mathcal{O}(\mathbf{A},\mathbf{C})$

$$\mathcal{O}(\mathbf{A},\mathbf{C}) = \begin{bmatrix} \mathbf{C} \\ \mathbf{CA} \\ \mathbf{CA}^2 \\ \vdots \\ \mathbf{CA}^{i-1} \end{bmatrix}. \qquad (11)$$

The observability Gramian can be obtained from the following equation

$$\mathcal{Q} = \mathcal{O}_\infty(\mathbf{C},\mathbf{A}))_\infty^T(\mathbf{C},\mathbf{A}) = \sum_{i=0}^{\infty} (\mathbf{A}^T)^i \mathbf{C}^T \mathbf{C}\mathbf{A}^i. \qquad (12)$$

B. Computation of Balancing Transformations

In general, a state coordinate transformation produces an equivalent model in another coordinate system. Using the transformation matrix $\mathbf{T} \in \mathbb{R}^{N\times N}$ the state-space model can be written as

$$\frac{\mathrm{d}\overline{\psi_i}(\mathrm{t})}{\mathrm{dt}} = \mathbf{T}\mathbf{A}\mathbf{T}^{-1}\overline{\psi}_i(t) + \mathbf{T}\mathbf{B}\mathbf{u}(t), \qquad (13)$$

$$y_i(t) = \mathbf{C}\mathbf{T}^{-1}\overline{\psi_i}(t), \qquad (14)$$

in which $\overline{\psi_i}(t) = \mathbf{T}\psi_i(t)$. The associated Gramians $\overline{\mathcal{P}}$ and $\overline{\mathcal{Q}}$ satisfy the following relationships

$$\overline{\mathcal{P}} = \mathbf{T}\mathcal{P}\mathbf{T}^T \quad \text{and} \quad \overline{\mathcal{Q}} = \mathbf{T}^{-T}\mathcal{Q}\mathbf{T}^{-1},$$

which gives

$$\overline{\mathcal{P}\mathcal{Q}} = \mathbf{T}\mathcal{P}\mathcal{Q}\mathbf{T}^{-1}.$$

By computing a Cholesky factorization of $\mathcal{P} = \mathbf{U}\mathbf{U}^T$ and $\mathcal{Q} = \mathbf{L}\mathbf{L}^T$ and a singular value decomposition of $\mathbf{U}^T\mathbf{L} = \mathbf{Z}\Sigma\mathbf{Y}^T$, it can be shown that setting

$$\mathbf{T} = \Sigma^{-1/2}\mathbf{Y}^T\mathbf{L}^T \quad \text{and} \quad \mathbf{T}^{-1} = \mathbf{U}\mathbf{Z}\Sigma^{-1/2}$$

leads to

$$\overline{\mathcal{P}} = \overline{\mathcal{Q}} = \mathrm{diag}(\sigma_1, \sigma_2 ..., \sigma_\mathrm{N}),$$

where $\sigma_1 \leq \sigma_2 \leq ... \leq \sigma_N$ [12]. Since the eigenvalues are coordinate independent, this gives the following so-called Hankel singular values

$$\sigma_i = \sqrt{\lambda_i(\mathcal{P}\mathcal{Q})} = \sqrt{\lambda_i(\overline{\mathcal{P}\mathcal{Q}})}, \qquad i = 1, 2, ..., N. \qquad (15)$$

It is important to note that the ith Hankel singular value σ_i can be interpreted as the energy contribution of the ith component of the balanced state to the input/output behavior of the system. If the Hankel singular values decrease rapidly, this means that the $\sigma_i \approx 0$ corresponds to the unreachable sets. Then, the system behavior is almost fully determined by the first few balanced states with $\sigma_i > 0$ [15]. Most of the model order reduction techniques for large-scale systems are based on the Hankel singular values and controllability/ observability Gramian [9].

C. Numerical Results

According to the parameter estimation obtained from CRONOS and discussed in Section II-B, the input/output response for the ψ profile discretized by $N = 101$ is shown in Figure 6. In principle, outputs can be chosen appropriate to the measurement techniques available in ITER, which might bring an addition limitation in determining the observability Gramian. Here, we consider the magnetic flux $\psi_i(t)$ to be fully observable.

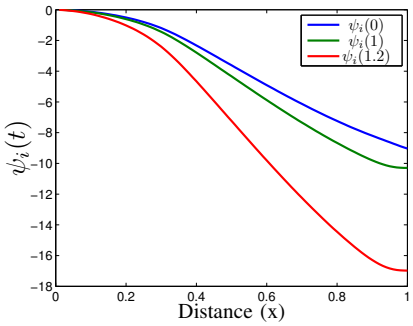

Fig. 6. Profiles of $\psi_i(t)$ according to (6)-(7) at $t = 0$, $t = 1$ms, and $t = 1.200$ms for $T_{\text{ped}} = 3$keV and $j_{\text{eccd}}(x)$ deposition at location $x = 0.3$.

The Hankel singular values according to (15) for deposition of $j_{\text{eccd}}(x)$ at three different locations are shown in Figure 7. As can be depicted, the Hankel singular values decrease rapidly. This means that not all $\psi_i(t)$ profiles are reachable from the chosen actuation strategy. The magnetic fluxes for $i > 30$ that correspond to $\sigma_{31}, \sigma_{30} ..., \sigma_{101}$ can be considered as unreachable, i.e., reachable with extremely high input energy.

Another important conclusion that can be drawn from the results shown in Figure 7 is related to the magnitude of the input energy for the given actuation strategies. The singular value σ_1 for the deposition of $j_{\text{eccd}}(x)$ at the location $x = 0.3$ is lower compared to σ_1 for the deposition at the location

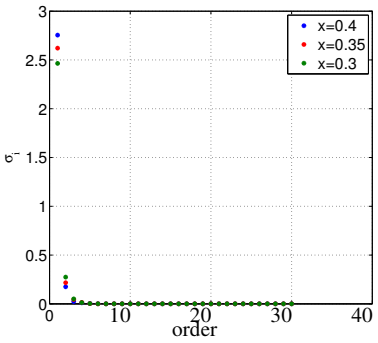

Fig. 7. The Hankel singular values of the first 30 largest singular values $\sigma_1, \sigma_2 ..., \sigma_{30}$ for $j_{\mathrm{eccd}}(x)$ deposition at $x = 0.3$, $x = 0.35$, and $x = 0.4$.

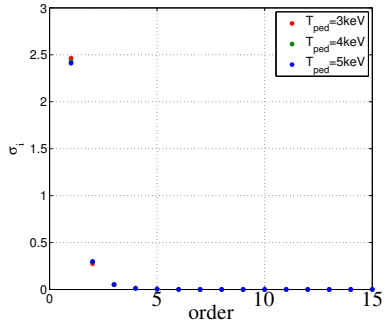

Fig. 8. The Hankel singular values of the first 30 largest singular values $\sigma_1, \sigma_2 ..., \sigma_{30}$ at T_{ped} at 3keV, 4keV, and 5keV.

$x = 0.4$. This suggest that the lower input energy is required for for the deposition of j_{eccd} closer to the center. This means that placing the $j_{\mathrm{eccd}}(x)$ deposition at $x = 0.3$ needs less input energy than the locations $x = 0.35$ and $x = 0.4$.

Furthermore, we also analyzed the influence of different T_{ped} on the singular values. Figure 8 illustrates the first 15 largest singular values as a function of T_{ped}. According to the results presented, we can conclude that the higher the pedestal temperature is set, the less input energy is required. Although the difference in the input energy for the given scenarios is negligible compared to the different actuation strategies.

IV. CONCLUSIONS

This paper presents a comprehensive framework for control-oriented modeling of the magnetic flux in ITER. The main feature of the proposed control-oriented model is that it is subject to less complex plasma conditions, such as the plasma resistivity, noninductive current density, and influence of the pedestal temperature, compared to the previous models. The control-oriented modeling approach to plasma fusion can be understood through possible input/output structures, which includes finding the most suitable actuation strategy for shaping the ψ-profiles with minimal input energy. In this paper, we have shown that the $j_{\mathrm{eccd}}(x)$ deposition at different locations influences the controllability Gramian, and consequently the input energy required to shape the ψ-profile. Furthermore, the controllability analysis has indicated that the system behaves as a model of much lower order, which should be considered in future work. Future work should also be devoted to validating the proposed model and extending this idea to other possible actuation strategies that can lead to more efficient operation of ITER.

V. ACKNOWLEDGMENTS

The authors gratefully acknowledge the support received from FOM-Institute for Plasma Physics Rijnhuizen, Association EURATOM-FOM, Trilateral Euregio Cluster for the generous help with the numerical part of this work and continuous exchange of ideas.

REFERENCES

[1] P. Moreau, O. Barana, S. Brémond, J. Bucalossi, E. Joffrin, E. Chatelier, D. Mazon, E. Witrant, E. Schuster, and M. Ariola, "Towards control of steady state plasma on Tore Supra," in *Proc. of IEEE Conference on Decision and Control, San Diego, CA, USA*, 2006.

[2] E. Synakowski, S. Batha, M. Beer, M. Bell, R. Bell, R. Budny, C. Bush, P. Efthimion, G. Hammett, T. Hahm *et al.*, "Roles of electric field shear and shafranov shift in sustaining high confinement in enhanced reversed shear plasmas on the TFTR tokamak," *Physical Review Letters*, vol. 78, no. 15, pp. 2972–2975, 1997.

[3] S. Ide, T. Fujita, T. Suzuki, T. Hatae, O. Naito, Y. Kamada, and M. Seki, "Combined non-inductive current drive in a high confinement reversed magnetic shear plasma at high normalized density in JT-60U," *Plasma Physics and Controlled Fusion*, vol. 44, p. L63, 2002.

[4] C. Challis, X. Litaudon, G. Tresset, Y. Baranov, A. Bécoulet, C. Giroud, N. Hawkes, D. Howell, E. Joffrin, P. Lomas *et al.*, "Influence of the q-profile shape on plasma performance in JET," *Plasma Physics and Controlled Fusion*, vol. 44, p. 1031, 2002.

[5] D. Moreau, D. Mazon, M. Ariola, G. Tommasi, L. Laborde, F. Piccolo, F. Sartori, T. Tala, L. Zabeo, A. Boboc *et al.*, "A two-time-scale dynamic-model approach for magnetic and kinetic profile control in advanced tokamak scenarios on JET," *Nuclear Fusion*, vol. 48, p. 106001, 2008.

[6] L. Laborde, D. Mazon, D. Moreau, A. Murari, R. Felton, L. Zabeo, R. Albanese, M. Ariola, J. Bucalossi, F. Crisanti *et al.*, "A model-based technique for integrated real-time profile control in the JET tokamak," *Plasma Physics and Controlled Fusion*, vol. 47, p. 155, 2005.

[7] E. Witrant, E. Joffrin, S. Brémond, G. Giruzzi, D. Mazon, O. Barana, and P. Moreau, "A control-oriented model of the current profile in tokamak plasma," *Plasma Physics and Controlled Fusion*, vol. 49, p. 1075, 2007.

[8] J. Artaud, V. Basiuk, F. Imbeaux, M. Schneider, J. Garcia, G. Giruzzi, P. Huynh, T. Aniel, F. Albajar, J. Ané *et al.*, "The CRONOS suite of codes for integrated tokamak modelling," *Nuclear Fusion*, vol. 50, p. 043001, 2010.

[9] P. Van Dooren, "Gramian based model reduction of large-scale dynamical systems," *Numerical analysis 1999*, p. 231, 2000.

[10] S. Guo and F. Romanelli, "The linear threshold of the ion-temperature-gradient-driven mode," *Physics of Fluids B: Plasma Physics*, vol. 5, p. 520, 1993.

[11] J. Citrin, J. Artaud, J. Garcia, G. Hogeweij, and F. Imbeaux, "Impact of heating and current drive mix on the ITER hybrid scenario," *Nuclear Fusion*, vol. 50, p. 115007, 2010.

[12] G. Golub and C. Van Loan, *Matrix computations*. Johns Hopkins University Press, 1996.

[13] D. Georges, "The use of observability and controllability gramians or functions for optimal sensor and actuator location in finite-dimensional systems," in *Decision and Control, 1995., Proceedings of the 34th IEEE Conference*, vol. 4. IEEE, 1995, pp. 3319–3324.

[14] B. Moore, "Principal component analysis in linear systems: Controllability, observability, and model reduction," *IEEE Transactions on Automatic Control*, vol. 26, no. 1, pp. 17–32, 1981.

[15] S. Shokoohi, L. Silverman, and P. Van Dooren, "Linear time-variable systems: Balancing and model reduction," *Automatic Control, IEEE Transactions*, vol. 28, no. 8, pp. 810–822, 1983.